Journal of Macromolecular Science, Part A
Publication details, including instructions for authors and subscription information:
http://www.informaworld.com/smpp/title~content=t713597274

Starburst Encapsulation of C_{60} by Multiple Hindered Two-Photon Absorptive Diphenylaminodialkylfluorene Arms

Robinson Anandakathir[a]; Loon-Seng Tan[b]; Long Y. Chiang[a]
[a] Department of Chemistry, University of Massachusetts Lowell, Lowell, MA [b] Air Force Research Laboratory, AFRL/MLBP, Wright-Patterson Air Force Base, Dayton, OH

To cite this Article Anandakathir, Robinson , Tan, Loon-Seng and Chiang, Long Y.(2007) 'Starburst Encapsulation of C_{60} by Multiple Hindered Two-Photon Absorptive Diphenylaminodialkylfluorene Arms', Journal of Macromolecular Science, Part A, 44: 12, 1265 — 1273
To link to this Article: DOI: 10.1080/10601320701606729
URL: http://dx.doi.org/10.1080/10601320701606729

Journal of Macromolecular Science®, Part A: Pure and Applied Chemistry (2007) **44**, 1265–1273

ISSN: 1060-1325 print/1520-5738 online
DOI: 10.1080/10601320701606729

Starburst Encapsulation of C_{60} by Multiple Hindered Two-Photon Absorptive Diphenylaminodialkylfluorene Arms

ROBINSON ANANDAKATHIR,[1] LOON-SENG TAN,[2] and LONG Y. CHIANG[1]

[1]*Department of Chemistry, University of Massachusetts Lowell, Lowell, MA*
[2]*Air Force Research Laboratory, AFRL/MLBP, Wright-Patterson Air Force Base, Dayton, OH*

The efficiency of nonlinear optical responses is highly influenced by the state of molecular assembly and aggregation. Introduction of bulky alkyl groups on an organic chromophore enhances its molecular dispersion in solution and, thus, simultaneous multiphoton absorptivity. Accordingly, sterically hindered fullerenyl chromophore triads $C_{60}(>\text{DPAF-C}_9)_2$ and pentads $C_{60}(>\text{DPAF-C}_9)_4$ were designed and synthesized for the use as optical limiting materials. Photoinduced molecular polarization is a crucial parameter for the enhancement of nonlinear optical responses. For this purpose, we synthesized these conjugates by attaching one or several diphenylaminofluorene moieties to methano[60]fullerene via a covalent keto linkage. The motif increases electronic interactions of DPAF-C_n rings with the C_{60} cage in close vicinity. Synthesis of $C_{60}(>\text{DPAF-C}_9)_n$ (n = 1, 2, or 4) was carried out by a four-step reaction procedure starting from 2-bromofluorene via dialkylation at C_9 position of fluorine ring and followed by attachment of a diphenylamino group at C_2 position of dialkylated fluorene, acylation of α-bromoacetyl group at C_7 position of diphenylaminodialkylfluorene, and subsequent Bingel cyclopropanation of DPAF-acyl bromide with C_{60}. All C_{60}-DPAF-C_n derivatives were fully characterized by various spectroscopic analyses. Molecular compositions of these conjugates were clearly confirmed by MALDI-TOF mass spectra. A method of relative proton counting was applied on the samples of complex $C_{60}(>\text{DPAF-C}_9)_2$ and $C_{60}(>\text{DPAF-C}_9)_4$ derivatives using DABCO as an internal standard for the calibration of proton integration in ^{1}H-NMR spectroscopic analyses.

Keywords: C_{60} chromophores; diphenylaminofluorene; multiadducts; nonlinear optical materials

1 Introduction

In recent years, synthetic approach and study of fullerene-based light harvesting derivatives have been proposed and attracted much attention due to their unique electronic, optical, and nonlinear optical properties (1–5). In the structure of these derivatives, fullerene cage serves as an electron acceptor (A) moiety while other organic electron-rich subunits, such as porphyrins, diphenylaminofluorenes (DPAF-C_n), and pyrrolidines, serve as donor (D) components (6–8). To achieve efficient harvesting of light energy, several research groups developed a numerous number of extended π-conjugated polymers (1), star-shaped molecules (9), nanoscaled molecules (10), and D-A systems containing multiple donor and acceptor subunits (6). One of the challenging tasks in fullerene functionalization chemistry is to synthesize highly efficient two-photon absorptive derivatives with covalent bonding of several chromophores without altering and disrupting the overall π-conjugation and electronic properties of the fullerene cage. Any one or two attachment(s) of the addend(s) on a C_{60} cage converts one double-bond into a single-bond moiety on the spherical ring structure. Attachment of multiple addends may result in removal of several conjugative fullerenyl olefins from the pristine C_{60} structure that reduces its electron-accepting capability. In general, the loss of 2–3 fullerenyl olefins may not lead to significant change of the first electrochemical reduction potential of the derivative as compared with that of C_{60}. However, a higher number of disrupted fullerenyl olefins than three in the structure of the derivative will experience a sharp increase of the reductive potential toward a more negative value required for uptake of the electrons. In this context, many functionalization chemistry were developed to selectively incorporate the addends with high regio- or stereoselectivity to retain or tune the optical properties of the resulting fullerenes (11). Recently, much effort was taken to investigate

Address correspondence to: Long Y. Chiang, Department of Chemistry, University of Massachusetts Lowell, Lowell, MA 01854. Tel.: (978)-934-3663; Fax: (978)-934-3013; E-mail: long_chiang@uml.edu

the structural relationship of multi-functionalized C_{60} adducts in a well-defined three-dimensional nanostructure (12−15) to their physical properties. Accordingly, these fullerenyl multi-adducts were synthesized by a stepwise addition method. Immediately after the monoadduct formation, addition of the second addend may not be regioselective that leads to formation of a number of possible bisadduct regioisomers as a product mixture. Further addition of more addends on the same C_{60} cage produces an even higher number of isomeric products, including regioisomers each with the same quantity of addends and mixed-multiads each with a different number of addends. Therefore, chromatographic separation and purification of these complex mixture products are insufficiently effective for a single compound isolation. To circumvent this complexicity, the tether-directed chemistry was employed to enhance better regioselectivity during the synthesis using a higher degree of functionalization (16, 17) that gave a less number of isomers. Alternatively, highly sterically hindered functional groups were used to induce a likely even distribution of functional attachments surrounding the cage surface by the simple size-effect. An example was provided by remarkably selective formation of fullerene derivatives by *trans*-1-adducts, which directed the subsequent addends to the equatorial belt (11). Based on this approach, hexakis-adducts of C_{60} were synthesized *via* their corresponding C_{60} tetrakis-adduct using terpyridylglycine and pyridylglycine (8) as the functional substrates.

In the present study, we applied highly fluorescent diphenylaminodialkylfluorene (DPAF-C_n) units as electron donor components in C_{60}-*keto*-donor structural assemblies, where DPAF-C_n acts as an antenna for efficient light harvesting in the visible region. One example of C_{60}-*keto*-donor dyad 7-(1,2-dihydro-1,2-methanofullerene[60]-61-carbonyl)-9,9-di(3,5,5-trimethylhexyl)-2-diphenylaminofluorene, $C_{60}(>$DPAF-$C_9)$, and its related bisadduct $C_{60}(>$DPAF-$C_9)_2$ were reported as highly two-photon absorbing (2PA) materials with large 2PA absorption cross sections (14). It became our interest in evaluation of structural relationship in terms of molecular branching to the enhancement of simultaneous two-photon absorbption cross sections and excited state properties. Specifically, we designed a new series of starburst C_{60}-*keto*-DPAF assemblies using multiple DPAF-C_n chromophore addends to encapsulate the molecular cage of C_{60}. In this case, a number of sterically hindered DPAF-C_n pendants are placed on a relatively small C_{60} using the method reported previously for the preparation of C_{60} ($>$DPAF-C_9) (18) with modification of fullerene cyclopropanation reaction conditions and the quantity of DPAF-C_n precursor reagent applied.

2 Experimental

Reagents of tris(dibenzylideneacetone)dipalladium 0, *rac*-2,2′-bis(diphenylphosphino)-1,1′-binaphthyl (BINAP), 2-bromofluorene, and all other chemicals were purchased from Sigma-Aldrich Chemicals. Infrared spectra were recorded as KBr pellets on a Thermo Nicolet 370 series FT-IR spectrometer. UV-Vis spectra were recorded on a Perkin-Elmer Lambda-9 UV/VIS/NIR spectrometer. ^{1}H-NMR and ^{13}C-NMR spectra in solution were taken on Bruker Avance Spectrospin-500 spectrometer. Fluorescence spectra were collected on a FLUOROLOG (ISA Instruments) spectrofluorometer. Mass spectroscopic measurements were measured by using positive ion matrix-assisted laser desorption ionization (MALDI−TOF) technique on a micromass M@ LDI-LR mass spectrometer. In a typical measurement, two fractions (100 μl) each from the solution of $C_{60}(>$DPAF-$C_9)_x$ (1.0 mg) in chloroform (1.0 ml) and the matrix solution of α-cyano-4-hydroxycinnamic acid (10 mg) in acetone (1.0 ml) were mixed together. From this sample-matrix mixture, a small quantity (2.0 μl) was taken and deposited on the stainless steel sample target plate, dried, and, subsequently, inserted into the ionization source of the instrument. The resulting sample blended or dissolved in the matrix material was irradiated by nitrogen UV laser at 337 nm with 10 Hz pulses under high vacuum. MALDI mass spectra were acquired in reflection mode. Each spectrum was produced by averaging 10 laser shots; at least 25 spectra were acquired from different regions of the sample target. Mass ion peaks were identified for the spectrum using the MassLynx v4.0 software.

2.1 Synthesis of 7-α-bromoacetyl-9,9-di(3,5,5-trimethylhexyl)-2-diphenylaminofluorene (4)

A modified literature procedure was used for this synthesis (18, 19). A solution of 9,9-di(3,5,5-trimethylhexyl)-2-diphenylaminofluorene **3** (1.4 g, 2.4 mmol) in 1,2-dichloroethane (30 ml) was added to the aluminum chloride suspension (1.12 g, 8.4 mmol, 3.5 equiv.) in 1,2-dichloroethane (50 ml) at 0°C. The compound α-bromoacetyl bromide (0.25 ml, 6.5 mmol) was then added dropwise to the mixture over a period of 5.0 min while maintaining the reaction temperature between 0−10°C. The mixture was slowly warmed to room temperature and stirred for an additional 8.0 h. It was quenched by the slow addition of icy cold water (100 ml) while maintaining the temperature below 45°C. The organic layer was separated, washed with dil. HCl (1.0 N, 50 ml), and water (50 ml, twice) in sequence. The organic layer was dried over magnesium sulfate and concentrated *in vacuo* to give the crude product as yellow oil. Further purification was made by column chromatography (silica gel) using a mixture of hexane−EtOAc (9:1) as the eluent. A chromatographic fraction corresponding to $R_f = 0.7$ on TLC [SiO_2, hexane: EtOAc (9:1) as the eluent] was isolated to afford 7-α−bromoacetyl-9,9-di(3,5,5-trimethylhexyl)-2-diphenylaminofluorene **4** as yellow viscous oil in 68% yield (1.2 g). The spectroscopic characteristics of **4** were identical to those data reported (20).

2.2 Synthesis of [60]fullerenyl tetraadducts C_{60}[methanocarbonyl-7-(9,9-di(3,5,5-trimethylhexyl)-2-diphenylaminofluorene)]$_4$, C_{60}(>DPAF-C_9)$_4$ 7a and 7b

C_{60} (550 mg, 0.76 mmol) and 7-α-bromoacetyl-(9,9-di(3,5,5-trimethylhexyl)-2-diphenylaminofluorene **4** (3.24 g, 4.6 mmol, 6.0 equiv.) were dissolved in anhydrous toluene (500 ml) under an atmospheric pressure of nitrogen. The reaction mixture was stirred at ambient temperature, resulting in a clear solution. To the solution, 1,8-diazabicyclo[5.4.0]undec-7ene (DBU, 850 mg, 5.5 mmol, 7.2 equiv.) was added and stirred at room temperature for a period of 8.0 h. Solid particles in the solution were filtered off and washed with toluene. The combined filtrate was concentrated to a volume of 50 ml. To this concentrated liquid was added methanol (100 ml) to effect precipitation of the crude products, which were isolated by centrifugation. Two major fractions were collected by column chromatography (silica gel) and subsequently repurified separately on preparative TLC plates [SiO_2, 2000 μm layer thickness, using a solvent mixture of hexane–toluene (4:1) for the less polar fraction and hexane–toluene (3:1) for the more polar fraction as the eluent]. During the PTLC separation, only a center narrow dense band was isolated to give [60]fullerenyl pentaads. These two product fractions were identified to be the regioisomeric tetraadducts; C_{60}[methanocarbonyl-7-(9,9-di(3,5,5-trimethylhexyl)-2-diphenylaminofluorene)]$_4$ **7a**, corresponding to the chromatographic band at $R_f = 0.5$ on analytical TLC plate using hexane–toluene (2:3) as the eluent, as brownish solids in 18% yield (440 mg) and **7b**, corresponding to the chromatographic band at $R_f = 0.25$ on analytical TLC plate, as brownish solids in 7% yield (170 mg).

Spectroscopic data of the first tetraadduct **7a**: MALDI–MS (TOF) calcd for $^{12}C^1_{240}H^{14}_{220}N^{16}_4O_4$ m/z 3221.6; found, m/z 3228, 3227, 3226, 3225, 3224, 3223, 3222 (M^+), 2639, 2619, 2560, 2599, 2597, 2540, 2127, 2104, 2102, 1972, 1563, 1547, 1543, 1479, 1468, 1456, 1347, 878, 870, 857, 827, 629, 612, and 531; FT-IR (KBr) υ_{max} 3421 (br), 2952 (vs), 2924 (vs), 2866, 1681, 1595 (vs), 1493 (vs), 1465, 1421, 1377 (w), 1347 (w), 1277, 1200, 1156 (w), 1029, 819, 752, 697 (s), 525, and 475 cm^{-1}; ^{1}H-NMR (500 MHz, $CDCl_3$, ppm) δ 8.5–8.0 (m, 8H), 7.9–7.5 (m, 8H), 7.24 (m, 20H), 7.1–6.9 (m, 28H), 5.6–5.0 (m, 4H), 2.4–1.7 (m, 16H), 1.4–1.1 (m, 16H), and 1.1–0.5 (m, 120H).

Spectroscopic data of the second tetraadduct **7b**: MALDI–MS (TOF) calcd for $^{12}C^1_{240}H^{14}_{220}N^{16}_4O_4$ m/z 3221.6; found, m/z 3228, 3227, 3226, 3225, 3224, 3223, 3222 (M^+), 2785, 2770, 2757, 2755, 2754, 2753, 2731, 2730, 2680, 2658, 2622, 2599, 2145, 2130, 2128, 2106, 2105, 2104, 1974, 1972, 1958, 1067, 1003, 948, 947, 946, 827, 629, 612, and 531; FT-IR (KBr) υ_{max} 3434 (br), 2951 (s), 2924 (vs), 2864, 1683, 1594 (vs), 1492 (vs), 1466, 1420 (w), 1363 (w), 1316 (w), 1278, 1211, 1177 (w), 1089, 819, 752, 697 (s), 525, and 474 (br) cm^{-1}; ^{1}H NMR (500 MHz, $CDCl_3$, ppm) δ 8.6–8.1 (m, 8H), 7.9–7.5 (m, 8H), 7.24 (m, 20H), 7.11 (m, 20H), 7.03 (m, 8H), 5.6–4.9 (m, 4H), 2.2–1.8 (m, 16H), 1.4–1.1 (m, 16H), and 1.1–0.4 (m, 120H).

3 Results and Discussion

Design and synthesis of starburst multiadducts of C_{60} were performed using multiple equivalents of two-photon absorptive dialkylated chromophores with a variation of the alkyl chain length and shape to tune the intermolecular aggregation tendency of chromophore components in highly concentrated solutions. A high concentration of the C_{60}-DPAF-C_n samples at 10^{-3}–10^{-2} M is often necessary for the 2PA measurements to compensate the low population of simultaneous two-photon pumped excited states. The reason of low population arises from the competition of fast relaxation of the single-photon pumped DPAF-C_n moiety at energy equivalent to one-half of its HOMO-LUMO gap. Alternatively, a low concentration of the sample at 10^{-4}–10^{-3} M may be used for the same evaluation with the application of much higher laser irradiation power. However, that may, in term, induce complication of the thermal scattering effect and sample decomposition. Therefore, steric control of chromophore structure to increase the intermolecular physical barrier and minimize molecular aggregation while maintaining the intramolecular co-planarity between conjugated donor and acceptor components becomes crucial in the high concentration measurement. Accordingly, we applied highly hindered 3,5,5-trimethylhexyl (C_9) groups each with several methyl branches in the chain to enhance the molecular

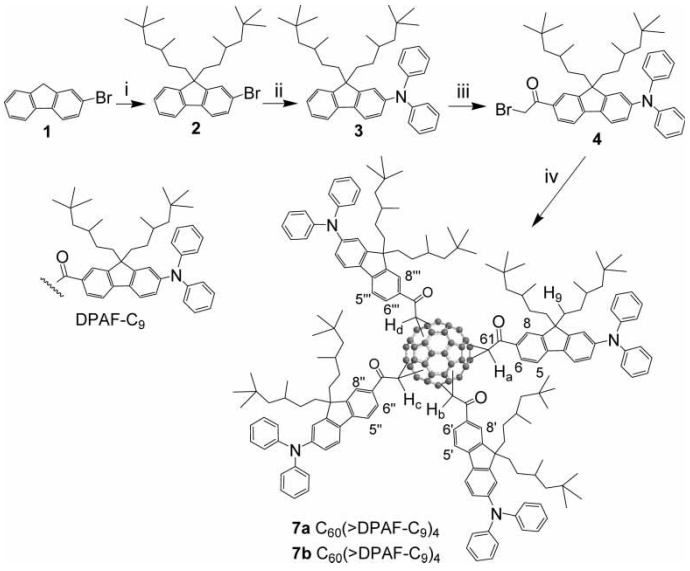

Sch. 1. Reagents and the reaction conditions: i) $(CH_3)_3CCH_2CH(CH_3)CH_2CH_2$-OMs, *t*-BuOK, THF, 10°C–rt, 15 h; ii) diphenylamine, tris(dibenzylideneacetone) dipalladium(0) (cat.), *rac*-BINAP (cat.), *t*-BuONa, toluene, reflux, 8.0 h; iii) bromoacetyl bromide, $AlCl_3$, $ClCH_2CH_2Cl$, 0°C to rt, 8.0 h; iv) C_{60}, DBU, toluene, rt, 8.0 h.

separation of diphenylaminodialkylfluorene (DPAF-C_n) chromophores, leading to proposed conjugated nanostructures of $C_{60}(>\text{DPAF-C}_9)_n$. Synthetic procedures for the preparation of $C_{60}(>\text{DPAF-C}_9)_n$ were outlined in Scheme 1. It followed previously reported detailed experimental reaction conditions for the synthesis of a fullerene dyad $C_{60}(>\text{DPAF-C}_9)$ **5**, 7-(1,2-dihydro-1,2-methanofullerene[60]-61-carbonyl)-9,9-di(3,5,5-trimethylhexyl)-2-diphenylaminofluorene, and the triads $C_{60}(>\text{DPAF-C}_9)_2$ **6**, C_{60}[methanocarbonyl-7-(9,9-di(3,5,5-trimethylhexyl)-2-diphenylaminofluorene)]$_2$ with modification (18).

Synthetically, as shown in Scheme 1, intermediate precursor synthon **2** was conveniently prepared from commercially available 2-bromofluorene **1** by dialkylation reaction with 3,5,5-trimethylhexyl (C_9) mesylate in tetrahydrofuran in the presence of potassium *t*-butoxide at 0°C to ambient temperature for 24 h. Subsequently, diphenylamination of **2** was carried out by Buchwald's procedure using diphenylamine as a reagent, *tris*-(dibenzylideneacetone) dipalladium 0 as a catalyst, *rac*-2,2′-bis(diphenylphosphino)-1,1′binaphthyl (BINAP) as a ligand, and sodium *t*-butoxide as a base in toluene at refluxing temperatures for a period of 12 h under an atmospheric pressure of nitrogen. The reaction yielded the corresponding product 9,9-di(3,5,5-trimethylhexyl)-2-diphenylaminofluorene **3** in high yield. Conversion of the structure **3** to the key precursor synthon **4** was carried out by Friedel-Crafts acylation and often encountered some difficulties in reproducing the same product yield. Apparently, reaction efficiency of this step depends highly on the quantity of aluminum chloride used, the reaction temperature, and the control of side-reactions. Many attempts were made to optimize the reaction conditions for producing a high yield of the desirable product. In a modified procedure, a relatively large quantity of aluminum chloride (3.5 equiv.) was found to be necessary in the reaction with α-bormoacetyl bromide in 1,2-dichloroethane at 0°C to ambient temperature for a period of 8 h to afford the corresponding product 7-α − bromoacetyl-9,9-di(3,5,5-trimethylhexyl)-2-diphenylaminofluorene (α-BrDPAF-C_9) **4**, as yellow viscous oil in 68% yield after column chromatography [silica gel, hexane–EtOAc, 9:1, $R_f = 0.7$ on thin-layer chromatography (TLC)] purification. Addition of DPAF-C_9 donor units to the fullerene cage for conversion of the intermediate **4** to the corresponding fullerene dyad $C_{60}(>\text{DPAF-C}_9)$ **5** and triads $C_{60}(>\text{DPAF-C}_9)_2$ **6** followed the reaction conditions of Bingel cycloproanation in toluene in the presence of 1,8-diazabicyclo[5.4.0]undec-7-ene (DBU, 1.1 equiv.) at ambient temperature for 5.0 h. Separation and purification of **5** and **6** were carried out by column chromatography (silica gel) using a solvent mixture of hexane–toluene (2:3) as the eluent. The first chromatographic band corresponding to $R_f = 0.85$ on TLC (SiO_2) plate was found to be the dyad **5** as brown solid in a yield of 65–70% (calculated based on the recovered C_{60}). The second chromatographic band corresponding to $R_f = 0.7$ on TLC plate gave the second product identified to be the triads **6** as brown solids in a yield of 9% (calculated based on the recovered C_{60}). Further purification of **6** was made on preparative TLC plates with the major narrow chromatographic band isolated at $R_f = 0.73$ using a solvent mixture of hexane–toluene (2:3) as the eluent.

Extension from the linear donor-acceptor structure **1** to the branched structure A-$(D)_n$ was achieved by the attachment of multiple equivalents of the donor component to C_{60}. In general, similar reaction conditions were applied for the synthesis of precursor intermediates **2**, **3**, and α-BrDPAF-C_9 **4** prior to the last synthetic step of Bingel cycloproanation. Modification of the latter reaction for the preparation of starburst $C_{60}(>\text{DPAF-C}_9)_n$ was made by using more than five equivalents of α-BrDPAF-C_9 per fullerene cage. As a matter of fact, application of two or three equivalents of the bromocompound **4** in the reaction may lead to the formation of bisadducts, trisadducts, and even possible tetraadducts in a lesser extend. For the purpose of enhancing the selectivity on a higher multiadduct yield in the products, we assumed that the highest possible number of bulky DPAF-C_9 donors to be attached on one C_{60} cage is six. Therefore, it is reasonable to apply 6.0 equivalents of α-BrDPAF-C_9 in the reaction with C_{60}. The experiment was carried out by stirring C_{60} with **4** in toluene in the presence of DBU (6.6 equiv.) at ambient temperature for a period of 8.0 h. Proceeding the reaction was followed by observation of the disappearance of corresponding chromatographic spots for the dyad $C_{60}(>\text{DPAF-C}_9)$ and triads $C_{60}(>\text{DPAF-C}_9)_2$, revealing their presence in a minimum quantity. At the end of the reaction, a similar workup procedure to that of $C_{60}(>\text{DPAF-C}_9)$ synthesis was used. Resulting crude product mixtures were subjected to the chromatographic separation and purification. Consequently, four chromatographic spots were identified on an analytical TLC plate each in a different quantity as estimated by spot intensity on the plate. Among them two most intense bands were collected by column chromatographic separation and further purified by the use of preparative TLC plates (SiO_2) with a solvent mixture of hexane–toluene (2:3) as the eluent. Isolation of these two narrow major bands afforded the corresponding C_{60}-DPAF-C_n multiadducts as follows. The first less polar fraction corresponding to the chromatographic spot at $R_f = 0.5$ on a TLC plate was identified to be the tetraadduct $C_{60}(>\text{DPAF-C}_9)_4$, C_{60} [methanocarbonyl-7-(9,9-di(3,5,5-trimethylhexyl)-2-diphenylaminofl-uorene)]$_4$ **7a**, in the form of a brown solid in 18% yield. The next major polar fraction corresponding to the chromatographic spot at $R_f = 0.25$ on an analytical TLC plate was found to be the second tetraadduct **7b** isolated as a brown solid in 7% yield. All other fractions amounted to a quantity equivalent to approximately 20% yield may be attributed from unidentified tetraads, pentaads, or hexaads.

The structure of all C_{60}-DPAF-C_n multiadducts was characterized by various spectroscopic methods. All spectra of previous well-characterized dyad $C_{60}(>\text{DPAF-C}_9)$ **5** provided useful references toward the characterization and identification of new starburst compounds **7a** and **7b**. In the optical absorption of pristine C_{60}, unique four sharp

characteristic harmonic peaks were observed at 530, 580, 1180, and 1430 cm^{-1} that can be used as the correlation of the existence of a sphere or semisphere cage exhibiting C_{60}-like fullerenyl π-conjugation. In the case of the fullerene monoadduct **5**, its structure consists of one DPAF-C_9 donor unit being attached on one-half sphere of the fullerene cage that leaves the other half-sphere untouched as a dissected C_{60} cage. Therefore, it is expectable to observe a half in intensity of infrared characteristics of C_{60} in the infrared spectrum of **5**. Interestingly, this proposed C_{60} bands do exist showing two sharp strong bands at 576 and 526 cm^{-1} (Figure 1a) in close resemblance to the peak position and relative absorption intensity to those of C_{60}. That revealed the monoaddition of one donor group on C_{60} will not disrupt optical absorption characteristics of the other half-sphere of the cage. Thus, the hypothesis becomes qualitatively useful for the prediction of region-locations of two DPAF-C_9 addends in the structure of bisadduct C_{60}(>DPAF-C_9)$_2$ **6**. As a result, similar two sharp bands at 576 and 526 cm^{-1} in the low wavenumber region were detected in low intensity (largely reduced from that of C_{60}) in the infrared spectrum of **6** (Figure 1b). It suggested the major regioisomer component of the product **6** bearing two DPAF-C_9 addends on the opposite half-sphere of the cage. It also indicated that two sterically hindered bulky 7-aceto-9,9-di(3,5,5-trimethylhexyl)-2-diphenylaminofluorene (DPAF-C_9, Scheme 1) components exhibit high tendency to separate from each other due to steric repulsion. The tendency resulted in the *trans*-regioisomer as the major bisadduct.

In the case of pentaads C_{60}(>DPAF-C_9)$_4$ **7**, these two low wavenumber peaks disappeared completely that implied four bulky DPAF-C_9 subunits being located around the full sphere of fullerene cage, as shown in Figures 1c (for **7a**) and 1d (for **7b**). Disappearance of pristine C_{60}-related characteristic bands was clearly indicative of disruption of perfect fullerenyl π-conjugation by four DPAF-C_9 attachments. In addition, IR spectra of DPAF-C_9 moieties in all adducts **5**, **6**, **7a**, and **7b** displayed nearly identical absorption bands including the band at 1683 cm^{-1} corresponding to the characteristic optical absorption of a keto group. This keto band showed a red-shift of about 50 cm^{-1} downfield from that of the normal ketone absorption range at 1725 cm^{-1}. It may be due to the influence of aromatic fluorene ring.

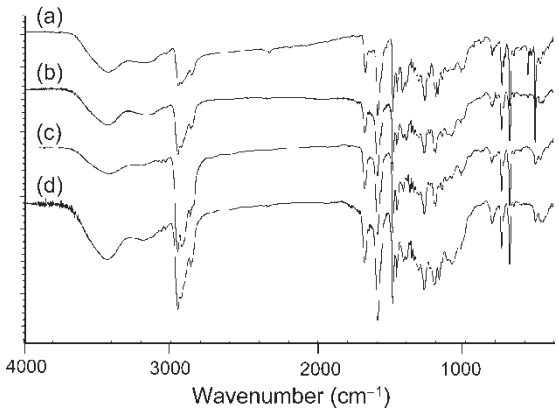

Fig. 1. Infrared spectra of (a) C_{60}(>DPAF-C_9) **5**, (b) C_{60}(>DPAF-C_9)$_2$ **6**, (c) C_{60}(>DPAF-C_9)$_4$ **7a**, and (d) C_{60}(>DPAF-C_9)$_4$ **7b**.

The proton NMR spectra of all adducts C_{60}(>DPAF-C_9)$_n$ in $CDCl_3$ were shown in Figure 2. The spectrum of α-BrDPAF-C_9 **4** displayed a singlet peak at δ 4.49, corresponding to the chemical shift of α-proton (H_α, next to the carbonyl group), and three groups of aromatic proton multiplet peaks observed at δ 7.65 (d, $J = 8$ Hz), 7.92 (d, $J = 8$ Hz), and 7.95 (dd, $J = 8$ Hz, $J = 1.6$ Hz) corresponding to chemical shifts of H_5, H_6, and H_8, respectively, of fluorene ring moiety. The chemical shift of α-proton of all C_{60}(>DPAF-C_9)$_n$ derivatives was found to shift downfield from that of **4**. For example, it appeared at δ 5.67 as a triplet-like signal in ^{1}H NMR spectrum (Figure 2a) of C_{60}(>DPAF-C_9) **5**. This downfield shift may be originated from long-range electronic interactions of α-proton with electron-withdrawing fullerenyl π-systems or cage current. Three types of aromatic protons in the structure of DPAF-C_9 moiety as H_5, H_6, and H_8 (Scheme 1) exhibited the corresponding peaks with the chemical shift at δ 7.82 (d, $J = 8$ Hz), 8.46 (d, $J = 8$ Hz), and 8.33 (s), respectively. Chemical shift of H_9 proton was found at δ 1.9–2.1 as a multiplet peak instead of a triplet that may be caused by the steric hindrance of neighboring phenyl groups.

As the structure extended to the triad C_{60}(>DPAF-C_9)$_2$ **6**, aromatic proton peaks appeared to be more complex in multiplet shape at δ 8.1–8.5 (4H), 7.41–7.8 (4H), 5.3–5.8 (2H), and 1.8–2.1 (8H) for the chemical shift of H_6–H_8/$H_{6'}$–$H_{8'}$, H_5/$H_{5'}$, α-protons, and H_9s protons, respectively (Figure 2b). Increasing complexicity in all peak

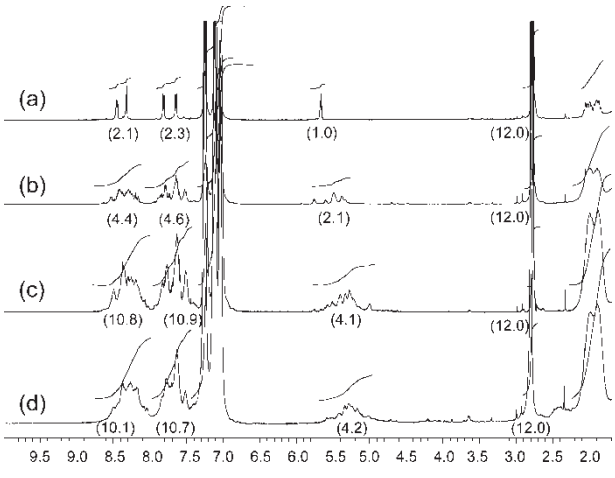

Fig. 2. ^{1}H-NMR spectra of (a) C_{60}(>DPAF-C_9) **5**, (b) C_{60}(>DPAF-C_9)$_2$ **6**, (c) C_{60}(>DPAF-C_9)$_4$ **7a**, and (d) C_{60}(>DPAF-C_9)$_4$ **7b** in $CDCl_3$ with relative integration values indicated. The values were calibrated by the use of an internal DABCO (singlet peak at δ 2.78) standard for the proton integration reference of 12H in the same concentration.

profiles may be reasoned by two sterically non-equivalent CH(DPAF-C_9) subunits that caused further peak splitting from the pattern detected for the dyad **5**. Evidently, two α-protons of **6** were correlated to two groups of proton peaks at δ 5.3–5.55 and 5.55–5.8 with a proton integration ratio of roughly 2.5:1.0. As concluded from the infrared spectrum of **6**, two possible regioisomers may be present with the major regioisomer, having two DPAF-C_n moieties located on the opposite side of the C_{60} sphere, in roughly 70% quantity and the minor regioisomer, having two DPAF-C_n moieties located on the same side of the C_{60} sphere, in roughly 30% quantity.

In the case of pentads, C_{60}(>DPAF-C_9)$_4$ **7a** and **7b**, α-proton peaks were located at δ 4.9–5.6 with each as a multiplet in the spectra of Figures 2d and 2e, respectively. A slightly upfield-shift from that of **6** was observed. In the structure of these two pentaads, four DPAF-C_9 moieties served as encapsulating pendants surrounding a fullerene cage with pronounced rigidity facing high steric hindrance to each other. That should restrict the free-rotation of each DPAF-C_9 pendant near the carbonyl bond and, thus, reduce the spectroscopic resolution of α-proton peak profiles for H_a, H_b, H_c, and H_d of **7a** and **7b**, as shown in Scheme 1. Similarly, broadened aromatic proton peaks in the region of δ 7.65–8.5 were grouped into three complex multiples each in a low ^{1}H–^{1}H coupling splitting resolution. However, chemical shifts and the peak profile of these peak groups were nearly identical to those of **5** and **6** indicating the same structural environment among **5**, **6**, and **7**, except increasing inhomogeneity of regio-location among DPAF-C_9 pendants on the surface of the cage.

Integration ratio of aromatic protons of the monoadduct, bisadducts, and tetraadducts at δ 7.0–8.6 can be applied for the correlation directly to their total number of aromatic protons in DPAF-C_9 subunits per molecule. To associate the exact proton counting to each other among different ^{1}H NMR spectra taken independently, we used a symmetrical molecule, 1,4-diazabicyclo[2.2.2]octane (DABCO), as an internal standard, prepared in the same concentration in each sample solution ($CDCl_3$). Compound DABCO shows a singlet proton peak at δ 2.78 for 12 symmetrical protons. In this study, a well-defined concentration of both DABCO and C_{60}(>DPAF-C_9)$_4$ sample was used with the spectra recorded as shown in Figures 2a–2d. Subsequently, exact numbers of the protons were calculated based on the relative integration ratio of the samples by using the following formula.

$$\frac{I_f}{N_{pf}}\frac{M_f}{m_f} = \frac{I_d}{N_{pd}}\frac{Md}{m_d}$$

where I_f is total proton integration of the compound, N_{pf} is the number of protons of the compound, M_f is the molecular weight of the compound, m_f is the weight of the compound sample used, I_d is total proton integration of DABCO, N_{pd} is the number of protons of DABCO, M_d is the molecular weight of DABCO, and m_d is the weight of DABCO sample used. For the sample solution (a) containing the monoadduct C_{60}(>DPAF-C_9) **5** (7.6 mg, 0.011 M) and DABCO (0.48 mg, 8.6×10^{-3} M) in $CDCl_3$ (0.5 ml), aromatic proton integrations with the value of 21.4 at δ 7.0–8.6 in ^{1}H-NMR spectrum (Figure 2a) gave the following results.

$$\text{Figure 2a for sample (a)}: \frac{I_f}{N_{pf}}\frac{M_f}{m_f} = \frac{I_d}{N_{pd}}\frac{M_d}{m_d} \rightarrow \frac{21.4}{N_{pf}}\frac{1345}{7.6\,\text{mg}}$$

$$= \frac{12.0}{12}\frac{112}{0.48\,\text{mg}}$$

That corresponds to the value of N_{pf} equivalent to 16.2 aromatic protons for **5** in good agreement with the theoretical value of 16. For the sample solution (b) containing the bisadduct C_{60}(>DPAF-C_9)$_2$ **6** (10.1 mg, 0.010 M) and DABCO (0.48 mg, 8.6×10^{-3} M) in $CDCl_3$ (0.5 ml), aromatic proton integrations with the value of 39.1 at δ 7.0–8.6 in ^{1}H NMR spectrum (Figure 2b) gave the following relationship:

$$\text{Figure 2b for sample (b)}: \frac{I_f}{N_{pf}}\frac{M_f}{m_f} = \frac{I_d}{N_{pd}}\frac{M_d}{m_d} \rightarrow \frac{39.1}{N_{pf}}\frac{1970}{10.1\text{mg}}$$

$$= \frac{12.0}{12}\frac{112}{0.48\,\text{mg}}$$

Calculation of the N_{pf} value led to a result of 32.6 aromatic protons for **6** in good agreement with the theoretical value of 32. Similarly, for the sample solution (c) containing the tetraadduct C_{60}(>DPAF-C_9)$_4$ **7a** (16.5 mg, 0.010 M) and DABCO (0.48 mg, 8.6×10^{-3} M) in $CDCl_3$ (0.5 ml), aromatic proton integrations with the value of 78.1 at δ 7.0–8.6 in ^{1}H-NMR spectrum (Figure 2c) allowed the following calculation to give a N_{pf} value as 65.3 aromatic protons for the structure **7a** in good agreement with the theoretical value of 64.

$$\text{Figure 2c for sample (c)}: \frac{I_f}{N_{pf}}\frac{M_f}{m_f} = \frac{I_d}{N_{pd}}\frac{M_d}{m_d} \rightarrow \frac{78.1}{N_{pf}}\frac{3220}{16.5\,\text{mg}}$$

$$= \frac{12.0}{12}\frac{112}{0.48\,\text{mg}}$$

The same operation for the sample solution (d) containing the tetraadduct C_{60}(>DPAF-C_9)$_4$ **7b** (16.5 mg, 0.010 M) and DABCO (0.48 mg, 8.6×10^{-3} M) in $CDCl_3$ (0.5 ml), aromatic proton integrations with the value of 77.1 at δ 7.0–8.6 in ^{1}H-NMR spectrum (Figure 2d) gave the N_{pf} result of 64.5 aromatic protons for the compound **7b** matching well with the theoretical value of 64. These proton correlation calculations clearly substantiated the structural composition of **5**, **6**, **7a**, and **7b** consisting of one, two, four, and four DPAF-C_9 addends, respectively, per C_{60} cage.

$$\text{Figure 2d for sample (d)}: \frac{I_f}{N_{pf}}\frac{M_f}{m_f} = \frac{I_d}{N_{pd}}\frac{M_d}{m_d}$$

$$\rightarrow \frac{77.1}{N_{pf}}\frac{3220}{16.5\,\text{mg}} = \frac{12.0}{12}\frac{112}{0.48\text{mg}}$$

Molecular weight of each C_{60}(>DPAF-C_9)$_n$ compound **5**, **6**, **7a**, and **7b** was confirmed by its positive ion matrix-assisted

laser desorption ionization mass spectrum (MALDI–MS) using α-cyano-4-hydroxycinnamic acid as the matrix material. Experimental conditions used for MALDI–MS spectrum data collection of the linear monoadduct **5** were applied as the method of calibration for the measurement of other multiadducts. Under these conditions and data elucidation, a group of molecular ion mass peaks were clearly detected at m/z 1346 for the mass of protonated **5** ion as MH^+ (Figure 3a). Subsequent MALDI–MS spectrum (Figure 3b) taken for the sample of $C_{60}(>\text{DPAF-C}_9)_2$ **6** showed a group of molecular ion mass peaks with the maximum peak intensity located at m/z 1972 which was assigned for the mass of protonated **6** ion (MH^+). In this group, the molecular ion mass peak (M^+, m/z 1971) and related isotope peaks of **6** at m/z 1973–1974 were clearly visible, as displayed in inset Figure 3e. It was followed by the loss of a CH_2(DPAF-C_9) (m/z 626) subunit showing a second group of mass ion peaks with the maximum peak intensity centered at m/z 1346, which is identical to the molecular mass of **5**. No other obvious intense fragmented mass ion peaks were detectable between these two masses indicating facile fragmentation and high stability of DPAF-C_9 chromophore arms under MALDI–MS conditions. Therefore, both Figures 3a and 3b provided solid evidence for the molecular mass of $C_{60}(>\text{DPAF-C}_9)$ and $C_{60}(>\text{DPAF-C}_9)_2$, respectively.

Utilizing the same technique of spectroscopic analysis, molecular mass of the starburst tetraadducts **7a** and 7**b** was characterized by their MALDI–MS spectrum. As the molecular weight of the sample increases above m/z 3000, the intensity of high molecular or fragmented mass ions becomes weaker significantly. The loss of peak resolution may go well underneath the detectable sensitivity range of the instrument. To compensate the difficulty, comparatively higher laser energy is necessary to overcome the low intensity of high mass ions. However, the use of high laser power is also accompanied by several adverse effects including low sample stability and the existence of additional contamination mass ion peaks in the spectrum collected. The latter may include the mass ion with one or two carbon units (m/z 15, 24, or higher, *etc*.) higher than the molecular mass of the sample studied. In the case of $C_{60}(>\text{DPAF-C}_9)_4$ **7a**, its MALDI–MS spectrum (Figure 3f) displayed a group of sharp mass ion peaks centered at m/z 3224 (MH_2^+), which corresponds to the mass of diprotonated $C_{60}(>\text{DPAF-C}_9)_4$, along with its molecular ion mass at m/z 3222 (M^+) and related isotope peaks at m/z 3223–3228. Additional major groups of mass fragmentation peaks were found at m/z 2599, 2104, 1972 and 1346 (Figure 3c). The former mass ion matches well with the mass of $C_{60}(>\text{DPAF-C}_9)_3$ arising from the loss of one CH(DPAF-C_9) group (m/z 625) from the molecular mass of **7a**. Consecutive loss of the second CH(DPAF-C_9) group led to the observed mass ion peak at m/z 1972 which was assigned for the $C_{60}(>\text{DPAF-C}_9)_2$ fragment. In close resemblance to Figures 3a and 3b, two strong low mass ion peaks were detected at m/z 612 and 629 for the mass of fragmented CH(DPAF-C_9) groups that supported the fragmentation pattern at the high mass region. These data confirmed undoubtedly the mass composition of **7a** as $C_{60}(>\text{DPAF-C}_9)_4$. Due to the use of high laser energy, additional mass ion groups were also visible at m/z 3247 $(M+2C)^+$ and 3263, which might be resulted from the addition of a CH_4 group to the former peak. Finally, the sharp mass ion peak at m/z 2104 was interpreted by the result of decarboxylation fragmentation of $C_{60}(>\text{DPAF-C}_9)_2$-($\alpha$-cyano-4-hydroxycinnamic acid) adduct.

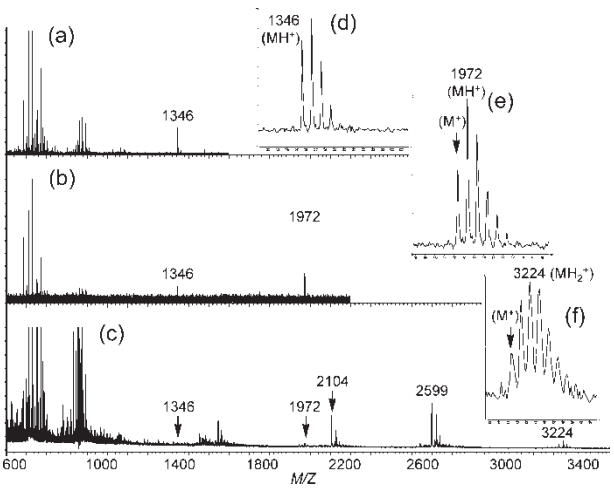

Fig. 3. Positive ion MALDI-TOF mass spectra of (a) $C_{60}(>\text{DPAF-C}_9)$ **5**, (b) $C_{60}(>\text{DPAF-C}_9)_2$ **6**, (c) $C_{60}(>\text{DPAF-C}_9)_4$ **7a**/**7b**. Insets: expanded spectra of (d) $C_{60}(>\text{DPAF-C}_9)$ **5**, (e) $C_{60}(>\text{DPAF-C}_9)_2$ **6**, and (f) $C_{60}(>\text{DPAF-C}_9)_4$ **7a**/**7b** at the group of MH^+ peaks.

Optical properties of photoresponsive chromophore are of importance for control of the excitation process to be carried out under laser irradiation. Difference in the chromophore-based linear optical absorption between $C_{60}>$ and DPAF-C_9 moieties allowed us to selectively exciting one chromophore component without affecting the others. This difference in the series of $C_{60}(>\text{DPAF-C}_9)_n$ conjugates was observed by their UV-Vis absorption spectra (Figure 4) showing three strong absorption bands centered at 257, 323, and 405 nm, as an example, for $C_{60}(>\text{DPAF-C}_9)$ **5**. The former two bands at 257 and 327 nm were assigned to the optical absorption of the fullerene cage while the later band at 405 nm was assigned to the DPAF-C_9 moiety. That correlates to the domination of optical absorption by the $C_{60}>$ cage in the structure of dyad **5** in the UV region while DPAF-C_9 moiety is the main photoresponsive component in the visible region. All spectra in Figure 4 fit well with the superimposed spectra of two independent chromophores as one combined molecular entity. Due to the fact that no shift of these three absorption bands was observed in the spectrum, it revealed no ground-state electronic interaction between $C_{60}>$ and DPAF-C_9 moieties in the dyad. That is

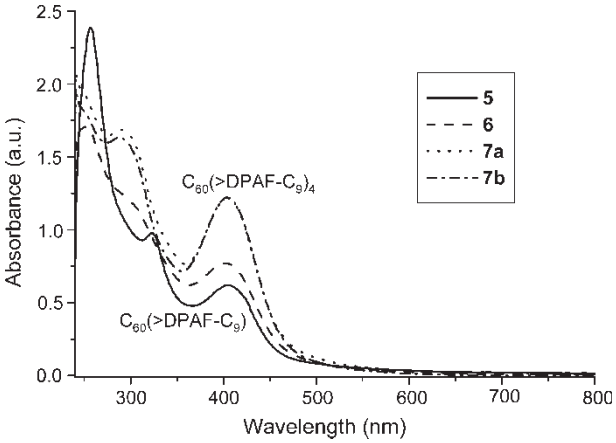

Fig. 4. UV-Vis Spectra of $C_{60}(>DPAF\text{-}C_9)$ **5**, $C_{60}(>DPAF\text{-}C_9)_2$ **6**, $C_{60}(>DPAF\text{-}C_9)_4$ **7a**, and $C_{60}(>DPAF\text{-}C_9)_4$ **7b** in chloroform in a concentration of 1×10^{-5} M.

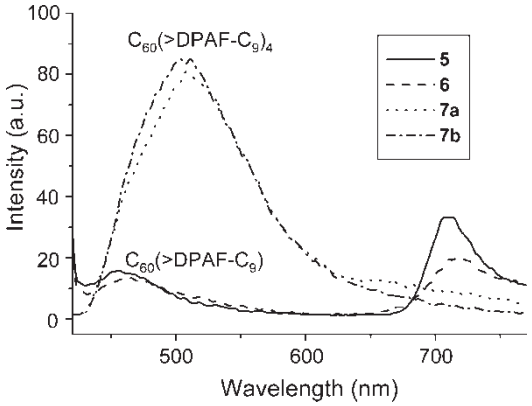

Fig. 5. Fluorescence Spectra of $C_{60}(>DPAF\text{-}C_9)$ **5**, $C_{60}(>DPAF\text{-}C_9)_2$ **6**, $C_{60}(>DPAF\text{-}C_9)_4$ **7a**, and $C_{60}(>DPAF\text{-}C_9)_4$ **7b** in chloroform upon photoexcitation at 400 nm.

also indicative of weak donor characteristics of DPAF-C_9 pendant.

Similarly, UV-Vis absorption spectra of $C_{60}(>DPAF)_2$ **6** and $C_{60}(>DPAF)_4$ **7a** and **7b** in Figure 4 displayed the optical absorption of DPAF moieties centered at 405 nm. Intensity of this band increases systematically with the increase of the number of DPAF moieties per fullerene cage from the dyad $C_{60}(>DPAF)$ to the pentaad $C_{60}(>DPAF)_4$ while the optical absorption of the fullerene cage remaining relative constant in solution of these adducts. That provided good evidence of the structural composition with $C_{60}(>DPAF)_4$ consisting of four DPAF-C_9 pendants. It was based on the estimation of absorption intensity increase from **5** to **7** at 405 nm using the increased intensity quantity from **5** to **6** at the same wavelength for the calculation base of one DPAF-C_9 unit.

Photoexcitation of $C_{60}(>DPAF\text{-}C_9)_n$ was performed in $CHCl_3$ by the application of irradiation at 400 nm, where DPAF-C_9 pendants are the main components responsible for several initial photoevents. As shown in Figure 5, immediately after irradiation of **5**, its fluorescence emission consists of two components with a weak fluorescence component covering from 430 to 530 nm and the second long wavelength weak fluorescence centered at 707 nm. This weak fluorescence revealed nearly quantitative quenching of DPAF-C_9 fluorescence by the fullerene cage. The quenching effect was caused by intramolecular electron and energy transfer processes occurring at various ultrafast time scales. The long wavelength fluorescence band at 707 nm is the characteristic emission of $^1C_{60}{}^*(>DPAF\text{-}C_9)$ with the lowest singlet excited energy estimated to be 1.76 eV. Interestingly, additional DPAF-C_9 pendant on the structure of **6** gave no enhancement of fluorescence emission at 707 nm. Instead, a slight decrease of this band in intensity was detected. When two more DPAF-C_9 pendants were attached to $C_{60}>$ leading to the structure of $C_{60}(>DPAF\text{-}C_9)_4$ **7a** and **7b**, intensity of the 707 nm band diminished further to a negligible level. One plausible explanation for the observed emission switching phenomena was given by an increasing ability of DPAF-C_9 donors to perform intramolecular electron-transfer to $C_{60}>$ cage via the transient $^1C_{60}^*(>DPAF\text{-}C_9)_n$ state as a quenching mechanism, leading to the formation of charge-separated ion-pairs $C_{60}^{-}\bullet(>DPAF^{+}\bullet\text{-}C_9)(>DPAF\text{-}C_9)_{n-1}$. Based on this hypothesis, the higher the number of DPAF-C_9 donors per $C_{60}>$ acceptor should give a faster rate or the higher probability for the intramolecular electron-transfer process to occur at the transient $^1C_{60}^*(>DPAF\text{-}C_9)_n$ state. Combination of this emission switching phenomena and fluorescence emission of **7a** and **7b** centered at 510 nm in high intensity were indicative of the existence of several possible transient states including $C_{60}^{-}\bullet(>DPAF^{+}\bullet\text{-}C_9)(>{}^1DPAF^*\text{-}C_9)(>DPAF\text{-}C_9)_2$, $C_{60}^{-}\bullet(>DPAF^{+}\bullet\text{-}C_9)(>{}^1DPAF^*\text{-}C_9)_2(>DPAF\text{-}C_9)$, and $C_{60}^{-}\bullet(>DPAF^{+}\bullet\text{-}C_9)(>{}^1DPAF^*\text{-}C_9)_3$.

4 Conclusions

A series of starburst C_{60}-*keto*-DPAF-C_n assemblies, such as $C_{60}(>DPAF\text{-}C_9)_n$ (n = 1, 2, or 4), were synthesized, purified, and characterized using sterically hindered 3,5,5-trimethylhexyl (C_9) groups for the physical barrier in separating diphenylaminodialkylfluorene (DPAF-C_n) chromophores with the attachment of multiple DPAF-C_n arms for encapsulation of the fullerene cage. Our synthetic strategy in utilizing a maximum number of DPAF-C_9 chromophore arms on one C_{60} cage to minimize the number probability of multiaddend variations and regioisomers formation allowed us to isolate a significant quantity and yield of the teraadduct products $C_{60}(>DPAF\text{-}C_9)_4$. Apparently, one C_{60} cage can not accommodate more than four bulky DPAF-C_9 pendants based on the fact that no noticeable yields of $C_{60}(>DPAF\text{-}C_9)_5$ and $C_{60}(>DPAF\text{-}C_9)_6$ were reachable. Remarkably, a starburst

structure constructed on a molecular C_{60} core enhanced the co-existence of intramolecular electron-transfer and energy-transfer processes from DPAF-C_9 moieties to the fullerene cage moiety via the transient $^1C_{60}{}^*(>\text{DPAF-C}_9)_n$ state. For example, this transient state took place from the intramolecular energy-transfer from the photoexcited $C_{60}(>{}^1\text{DPAF}^*\text{-C}_9)_n$ transient state. Subsequent intramolecular electron-transfer processes converted it to the formation of corresponding charge-separated ion-pairs $C_{60}^{-}\bullet(>\text{DPAF}^{+}\bullet\text{-C}_9)$ $(>{}^1\text{DPAF}^*\text{-C}_9)_m(>\text{DPAF-C}_9)_{n-m-1}$, giving the expected photophysical properties in good agreement with observed fluorescence emission spectra.

5 Acknowledgements

We thank Air Force Office of Scientific Research for funding under the contract number FA9550-05-1-0154.

6 References

1. Segura, J.L., Martin, N. and Guldi, D.M. (2005) *Chem. Soc. Rev.*, **34**, 31–47.
2. Guldi, D.M. and Prato, M. (2000) *Acc. Chem. Res.*, **33**, 695–703.
3. Guldi, D.M. and Kamat, P.V. *Fullerenes, Chemistry, Physics and Technology*. Kadish, K.M. and Ruoff, R.S. (eds.); Wiely-Interscience New York, 225–281, 2000.
4. Maggini, M. and Guldi, D.M. *Molecular and Supramolecular Photochemistry*. Ramamurthy, V. and Schanze, K.S. (eds.); Marcel Dekker: New York. Vol. 4, 149–196, 2000.
5. Eckert, J.-F., Nicoud, J.-F., Nierengarten, J.-F., Liu, S.-G., Echegoyen, L., Barigelletti, F., Armaroli, N., Ouali, L., Krasnikov, V. and Hadziioannou, G. (2000) *J. Am. Chem. Soc.*, **122**, 7467–7479.
6. Li, W.S., Kim, K.S., Jiang, D.L., Tanaka, H., Kawai, T., Kwon, J.H., Kim, D. and Aida, T. (2006) *J. Am. Chem. Soc.*, **128**, 10527–10532.
7. Padmawar, P.A., Canteenwala, T., Sarika, V., Tan, L.-S. and Chiang, L.Y. (2006) *J. Mater. Chem.*, **16**, 1–14.
8. Zhang, S., Lukoyanova, O. and Echegoyen, L. (2006) *Chem. Eur. J.*, **12**, 2846–2853.
9. Wang, J.L., Duan, X.F., Jiang, B., Gan, L.B. and Pei, J. (2006) *J. Org. Chem.*, **71**, 4400–4410.
10. Shirai, Y., Osgood, A.J., Zhao, Y., Kelly, K.F. and Tour, J.M. (2005) *Nano Lett.*, **5**, 2330–2334.
11. Krautler, B., Muller, T., Maynollo, J., Gruber, K., Kratky, C., Ochsenbein, P., Schwarzenback, D. and Burgi, H.B. (1996) *Angew. Chem. Int. Ed. Engl.*, **35**, 1204–1207.
12. Canteenwala, T., Padmawar, P.A. and Chiang, L.Y. (2005) *J. Am. Chem. Soc.*, **127**, 26–27.
13. Zhou, Z., Schuster, D.I. and Wilson, S.R. (2003) *J. Org. Chem.*, **68**, 7612–7617.
14. Padmawar, P.A., Rogers, J.O., He, G.S., Chiang, L.Y., Canteenwala, T., Tan, L.-S., Zheng, Q., Lu, C., Slagle, J.E., Danilov, E., McLean, D.G., Fleitz, P.A. and Prasad, P.N. (2006) *Chem. Mater.*, **18**, 4065–4074.
15. Marchesan, S., Da Ros, T. and Prato, M. (2005) *J. Org. Chem.*, **70**, 4706–4713.
16. Zhou, Z. and Wilson, S.R. (2005) *Current Organic Chemistry*, **9**, 789–811.
17. Nakamura, Y., Suzuki, M., Iami, Y. and Nishimura, J. (2004) *Org. Lett.*, **4**, 2797–2799.
18. Padmawar, P.A., Canteenwala, T., Tan, L.-S. and Chiang, L.Y. (2006) *J. Mater. Chem.*, **16**, 1366–1378.
19. Padmawar, P.A., Canteenwala, T., Sarika, V., Tan, L.-S. and Chiang, L.Y. (2004) *J. Macromol. Sci. A, Pure Appl. Chem.*, **41**, 1387–1400.
20. Tang, B.Z., Xu, H., Lam, J.W.Y., Lee, P.P.S., Xu, K., Sun, Q. and Cheuk, K.K.L. (2000) *Chem. Mater.*, **12**, 1446–1455.